Proceedings of NUMOS
Gent, 28-30 March 2007

Numos 2007, pp. 297–309

Investigation of the electronic properties of the recombination heterointerface in CGS/CIGS monolithic tandem solar cell

G. Černivec[1], M. Burgelman[2] F. Smole[1], M. Topič[1]

[1]Faculty of Electrical Engineering, University of Ljubljana

[2]Electronics and Information systems (ELIS), University of Gent

Abstract

We have investigated, by means of numerical simulation, the possible nature of the recombination heterointerface in the monolithic CGS (top)/CIGS (bottom) tandem solar cell. The results show that current transport by tunnelling might be of less importance. On the other hand, a good recombination junction can be achieved by a formation of a semi–metal at the back contact. It is proposed that a thin interlayer of $MoSe_2$, which is of semi–metallic nature, is introduced at the CGS back contact in order to have a good ohmic contact between the two cells in the tandem. Numerical simulation of the tandem structure reveals that there exists an optimal thickness of the top absorber. The most probable limitations of the efficiency of this tandem structure are a low open circuit voltage and a low fill factor.

1. Introduction

The idea of thin film tandem solar cells based on II–VI compound solar cells has been introduced more than two decades ago [1]. A logical evolution of the great success of single junction $Cu(In,Ga)Se_2$ (CIGS) thin film solar cells was the realization of a two–junction mechanically stacked tandem solar cell. A lot of experimental and theoretical research has been done on the semi–transparent top cell and of complete 4–terminal devices [2]–[7]. The main goals still remain the development of a semi–transparent top cell with AM1.5g efficiency above 17 %, and the formation of the monolithic interconnecting contact. The latter can be achieved in two ways: by making a tunneling recombination junction or by inserting an intermediate layer with work function close to the work function of the bottom cell.

Ideally the ohmic contact should be formed as a tunneling recombination junction, similar as in the a–Si tandem solar cell [8]. It would comprise a highly *p*–type doped back contact of the top cell and a highly *n*–type doped front contact of the bottom cell, and it should exhibit a high density of recombination centers (Figure 1). Although monocrystalline and polycrystalline CGS can be doped above 10^{19} cm^{-3} [9], [10] the CGS absorber in a

complete solar cell structure usually exhibits a much lower doping density, i.e. around 10^{16} cm^{-3} [11], [12].

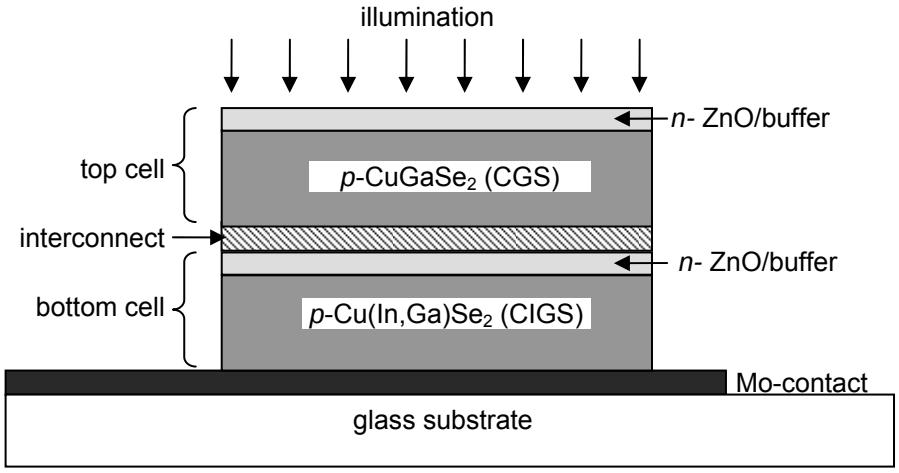

Figure 1 Schematic structure of a CIGS/CGS tandem solar cell, and the interconnection junction or layer between the cells. The terminology is that the interconnection layer is the 'back contact' of the top cell, and the 'front contact' of the bottom cell.

The intermediate layer should be a material with low optical absorption, appropriate work function and good chemical and thermal stability. Thin conductive oxides (TCO's) would be the ideal choice, if there were no inherent problems with the *p*–type doping [13]. However, transparent CIGS cells already achieved an efficiency higher than 12 %, using a 'normal' *n*–doped TCO as the back contact [14], [15]. This is surprising since the large band gap of the TCO produces a high blocking barrier (> 3 eV) in the valence band of the absorber, which should allow no hole current across.

However there are two possible ways to enable a hole current to flow: i) the photogenerated holes are able to tunnel through the part of the valence band barrier into the allowed states at the heterointerface and recombine with the bottom cell's photogenerated electrons (Figure 2) or ii) an additional thin layer is introduced at the heterointerface with the valence band of the top absorber overlapping with the TCO's conduction band resulting in a semi–metal formation (Figure 4). With the lowered band gap and high electron and hole concentrations, a high thermal recombination brings work functions of both materials close together and produces a good ohmic contact. We discuss both possibilities in section 2.

In section 3 we investigate the efficiency of the monolithic tandem solar cell under the AM1.5g solar spectrum and the influence of the top cell's absorber thickness. Thick top cell heavily screens the bottom cell which limits the short circuit current (J_{sc}) of the tandem. Thinning down the top absorber increases the J_{sc}, but decreases the fill–factor (*FF*). There exists an optimal thickness of the top cell's absorber layer but nevertheless the efficiency of the monolithic tandem does not surpass the efficiency of the CIGS bottom cell. We will discuss the reasons for this in section 4.

2. Recombination heterointerface

2.1 Tunneling to the interface states

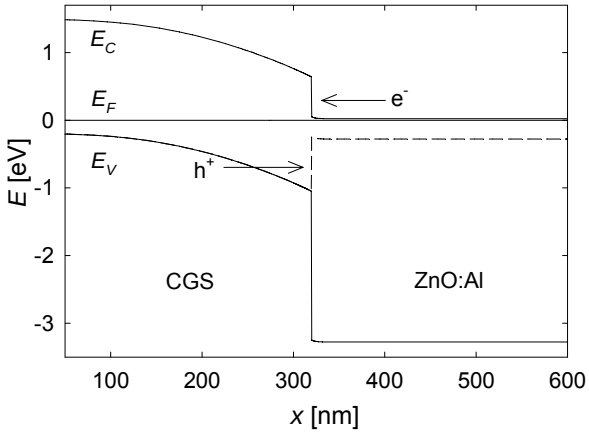

Figure 2 A two–layer *p*/*n* structure: a heterointerface between the top cell's CGS absorber and bottom cell's ZnO:Al window layer. The dashed line represents the states in the gap where a hole transport is allowed. A path for tunneling of holes from CGS to ZnO is indicated.

Figure 2 shows the possible band alignment in thermal equilibrium at the heterointerface contact between the top and the bottom solar cell. A wide depletion region, extending over 200 nm deep into the top cell's CGS absorber can be observed. Due to a mismatch in the band alignment, the band bending in equilibrium equals the built–in potential V_{bi}, given by

$$V_{bi} = \frac{1}{q} E_{G,\mathrm{CGS}} - \left(\chi_{\mathrm{ZnO}} - \chi_{\mathrm{CGS}}\right) - \left(\eta_p + \eta_n\right) \tag{1}$$

where the meaning of the symbols and their values are given in Table 1. The values of η_p and η_n are given for doping densities $N_A = 2\times10^{16}$ cm^{-3} in CGS and $N_D = 10^{18}$ cm^{-3} in ZnO, and literature values of the relevant effective

densities N_C and N_V. With the parameters of Table 1, V_{bi} = 0.9 V. As long as $N_A \ll N_D$, this band bending is almost completely over the CGS layer.

Table 1 Parameters of the energy band alignment at the CGS/ZnO heterointerface.

property	symbol	unit	*p*-CGS	*n*-ZnO
band gap	E_G	eV	1.69	3.3
electron affinity	χ	V	3.41	4.0
Fermi level to majority carrier band	η	V	0.18	0.02

Holes can be transported to the allowed gap states by the diffusion and/or by the tunnelling. But regarding the shape of the barrier (width 200 nm, height 0.9 eV), the tunnelling contribution is expected to be very small. In order to quantify the tunnelling contribution to the dark saturation current, we have varied the barrier in two ways. By increasing CGS the doping concentration N_A, both barrier width (equal to the depletion width in CGS) and the barrier height (equal to the fraction of the built–in voltage V_{bi} over the CGS layer) decrease, resulting in an increase of the barrier's tunnel transparency.

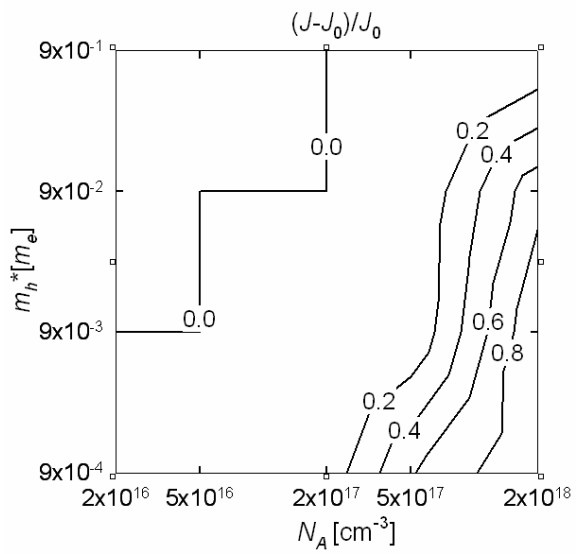

Figure 3 Dark current J due to tunnelling transport in the CGS/ZnO:Al structure. The ordinate is the relative increment of J above the reference dark current J_0, calculated with m_h = 0.73 m_e and $N_A = 2\times10^{16}$ cm^{-3}. The structure is not illuminated and reversely biased at $V = -0.3$ V.

By decreasing the hole effective mass (m^*_h), the barrier's transparency increases, since lighter holes are 'easier' to tunnel.

The dark current J was calculated with ASPIN2 [16]. Figure 3 shows the dark current increment ($J - J_0$) relative to the reference dark current J_0. The reference J_0 is calculated with the parameters from the upper–left corner: $m_h = 0.73\ m_e$ and $N_A = 2\times10^{16}$ cm^{-3} which are physically reasonable values for the CIGS material. By increasing the N_A to a very high value of 2×10^{18} cm^{-3} the depletion region shrinks to around 20 nm, and since the band bending then occurs also in ZnO:Al the barrier height lowers to 0.4 eV. There is only small relative increment of the J (upper–right corner of the Figure 2), most probably only due to the thermally activated hole current across the lowered barrier. In order to get a noticeable dark current increment, the m^*_h has to be lowered over three orders of magnitude (lower–right corner of Figure 3). The dark saturation current increment is modest, only by factor 2.

2.2 Recombination at the intermediate layer

Figure 4 shows the same CGS/ZnO:Al heterointerface structure, where an 'intermediate layer' was introduced by gradually transforming the semiconductor properties of a 20 nm thin layer at the ZnO:Al surface. The band diagram of the original structure is depicted by dashed lines. In a first transformation, the band gap of the 20 nm interlayer was decreased from 3.3 eV (value for ZnO) to 1.1 eV.

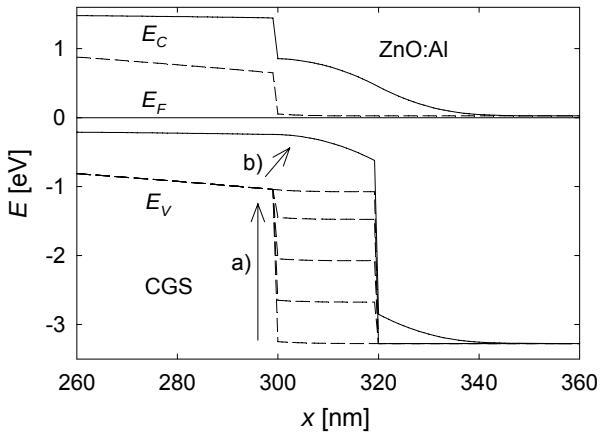

Figure 4 Introduction of the intermediate recombination layer by changing the properties of a 20 nm thick surface layer of ZnO:Al: a) the band gap was decreased from 3.3 eV to 1.1 eV (5 steps), b) then, the net doping was changed to acceptor acceptor-type, with density 10^{18} cm^{-3} (one step).

This is indicated with the arrow a) in Figure 4, and in dashed lines, too (there are only changes in the valence band). In a second transformation, the majority carrier type of the interlayer was changed by assigning it a net acceptor doping of 10^{18} cm^{-3}. This is indicated with arrow b), and the band diagram is shown in solid lines (changes in E_C and E_V). Figure 5 shows the corresponding dark *J–V* characteristics of the CGS/ZnO:Al structure with the formed interlayer.

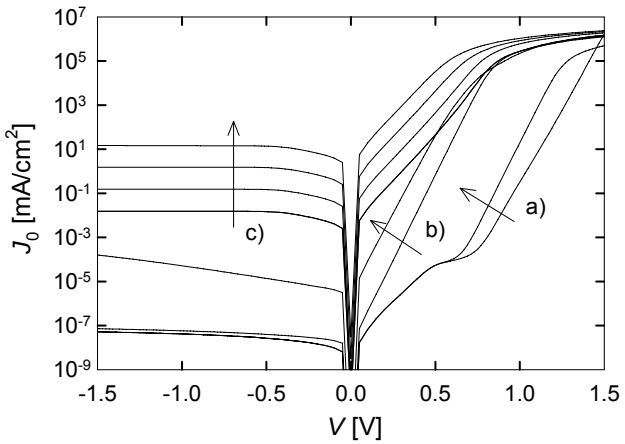

Figure 5 Dark *J–V* characteristics of the CGS/ZnO:Al structure. The arrows show the following processes of the transformation of the material parameters of the 20 nm surface of ZnO:Al: (a) lowering the band gap and (b) increasing the hole concentration. In (c), the capture cross–section of the interlayer defects is increased with three orders of magnitude, in 3 steps.

One can observe that the saturation current after the transformations a) and b) is still too low to form an efficient recombination contact. The dark reverse current should be comparable to the photogenerated current, as a rough approximation for an efficient recombination contact. In order to achieve a dark saturation current higher than the 10 mA/cm^2, the thermodynamical properties of the midgap defects in the interlayer have to be changed: the defect cross–sections are increased by 3 orders of magnitude from the geometrical cross–sections, as shown with arrow c) in Figure 5. Since this has low impact to the charge redistribution, there is no change in the band diagrams of Figure 4.

2.3 Nature of the recombination interlayer

In order to make an efficient contact between the top CGS and the bottom CIGS solar cell we had to transform a 20 nm thick surface layer of ZnO:Al

into a new material which differs from the original ZnO:Al material, because it has a) lower band gap (1.1 eV instead of 3.3 eV), b) a surface hole concentration of 2×10^{18} cm^{-3}, comparable to the electron concentration in the ZnO bulk, and c) a thousand times larger defect cross–section. Thus, this surface layer clearly is no longer ZnO, but it is a new semiconductor material. Another property is that it serves well as 'ohmic' contact between CGS and ZnO, i.e. it brings the quasi–Fermi energies E_{Fp} of CGS and E_{Fn} of ZnO very closely together (to only 50 meV difference, see Figure 6). This property, of having a single Fermi level $E_F = E_{Fn} = E_{Fp}$, is specific for metals. Since the interlayer thus exhibits both semiconductor and metallic properties, it can be characterized as a semi–metal.

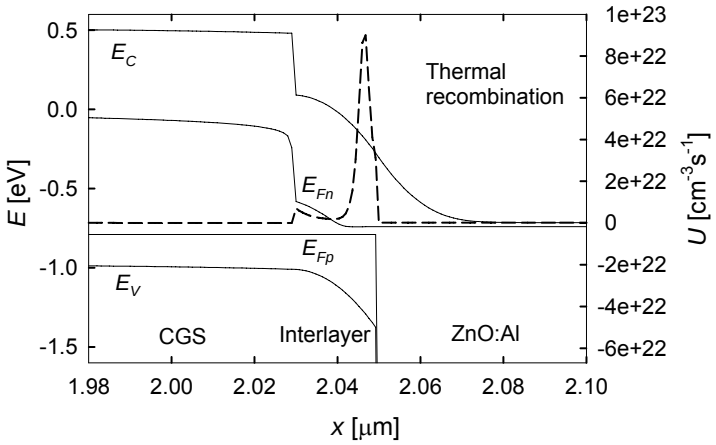

Figure 6 Detail around the CGS/ZnO heterointerface of the monolithic tandem solar cell, under AM1.5g illumination and with 0 V applied bias. The thermal recombination profile is shown in a dashed line and refers to the right axis.

Figure 6 shows a detail of the energy band diagram at the heterointerface/interlayer of the tandem structure, as described above. The quasi–Fermi energy difference over the interlayer is very small, around 50 meV only. Also, a very high thermal recombination may be observed at the interlayer. Thermal recombination indeed tends to bring the electron and hole distributions back to the thermal equilibrium, i.e. to equilibrate the hole quasi–Fermi energy with the electron quasi–Fermi energy into the single Fermi energy. To achieve such high thermal recombination, the defect cross–sections had to be increased with 3 decades from the geometrical cross–sections, i.e. the thermodynamical properties of the semiconductor were changed to form a semi–metal.

Molybdenum diselenide ($MoSe_2$) has been successfully used as an interlayer to form an efficient ohmic back contact: when formed between the CIGS and the molybdenum (Mo) back contact, the contact looses its Schottky–like nature [17], [18]. Also, when formed between the CIGS and ZnO, the back contact looses its rectifying nature [14], [15]. It seems that the $MoSe_2$ forms an efficient recombination junction with the bottom Mo metal or with *n*–type ZnO layers, and does not introduce rectifying properties with the *p*–type top CIGS layer: it behaves as a semi–metal. The measured band gap range (1.2 eV – 1.4 eV) and its thickness (15 nm – 30 nm) are also in good correlation with our numerical model.

3. Monolithic tandem solar cell

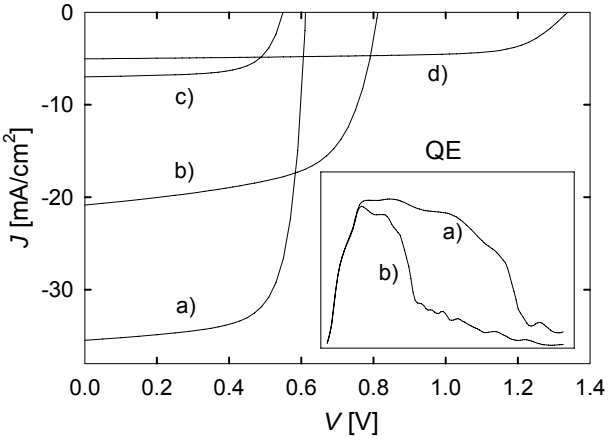

Figure 7 *J–V* characteristics of the AM1.5g illuminated structures: a) bottom cell, b) top cell, c) screened bottom cell and d) the tandem structure. Inset: $QE(\lambda)$ of a) and b).

To simulate a monolithic CGS/CIGS tandem structure, we use a $MoSe_2$ interlayer at the CGS/ZnO:Al heterojunction, with properties as described above. The material parameters of the bottom cell are taken from one of our previous models [19] with a 2 μm thick CIGS absorber layer and increased electron/hole mobilities. The same parameters are used for the top CGS cell, where the absorber layer is 1.6 μm thick and the band gap is increased to 1.69 eV. The optical simulator SunShine [20] is used to calculate the generation rate profile of the tandem structure under the AM1.5g solar spectrum illumination. Figure 7 shows the *J–V* simulations of the illuminated structures: a) the bottom CIGS solar cell alone: ZnO:Al/ZnO/CdS/CIGS/Mo, b) the top CGS solar cell with a transparent back contact alone: ZnO:Al/ZnO/CdS/CGS/$MoSe_2$/ZnO:Al, c) the screened bottom CIGS solar

cell, i.e. the illumination with the AM1.5g spectrum lowered for the top cell's absorbance, and d) the complete tandem solar cell. The inset of Figure 7 shows the quantum efficiencies of the bottom a) and the top b) solar cell.

The output solar cell parameters are compared in Table 2. The very low efficiency < 5 % of the tandem may be surprising at first but a glance at the short circuit current densities (J_{sc}) reveals the reason: the bottom solar cell is heavily screened by the top solar cell c).

Table 2 Output parameters of the simulated structures.

	Solar cell	J_{sc} [mA/cm^2]	V_{oc} [mV]	FF [%]	η [%]
a	Bottom CIGS	35.5	612	72.4	15.7
b	Top CGS	20.9	812	61.9	10.5
c	Screened bottom	6.98	549	68.1	2.61
d	Tandem	5.04	1340	71.0	4.78

Not enough electrons are photogenerated in the bottom cell to recombine all the photogenerated holes from the top cell, therefore the excessive holes are recombined in the top absorber and lost. The bottom solar cell is limiting the J_{sc}, but the reason for this resides in a too thick top cell absorber. Figure 8 shows the variation of the top solar cell's absorber thickness (W_{abs}).

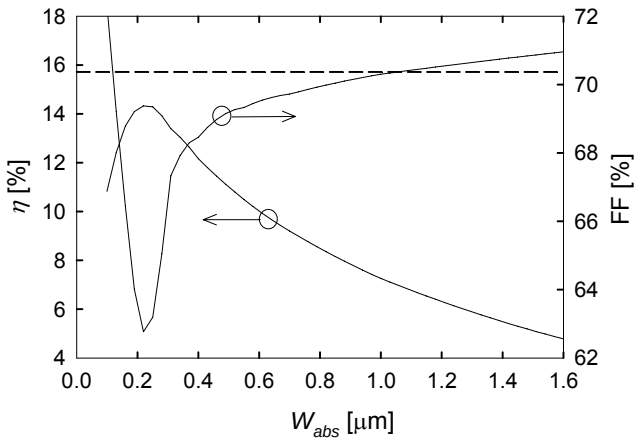

Figure 8 Dependence of the efficiency η of the tandem cell on the thickness of the CGS absorber of the top cell. For comparison, the dashed line shows the AM1.5g efficiency of the bottom CIGS cell. The short circuit current J_{sc} of the tandem is not presented here, but it has the same thickness dependence as $\eta(W_{abs})$, with a maximum value of $J_{sc,M} = 15$ mA/cm^2.

Thinning down the CGS absorber increases the short circuit current J_{sc} and the efficiency η of the tandem. The open circuit voltage V_{oc} increases only due the higher J_{sc}, but this increase is not significant. There is a maximum of the η slightly above $W_{abs} = 0.2$ μm. The maximum of η coincides with the maximum of J_{sc} and with the minimum of the fill factor *FF*. The efficiency drop for a thinner top cell absorber, $W_{abs} < 0.2$ μm, occurs from lowered absorption in the CGS absorber, which starts limiting the J_{sc} and the back contact recombination of the top cell's photogenerated electrons. The $MoSe_2$ interlayer comes to close the junction and photogenerated electrons start diffusing towards the back contact and recombining with the photogenerated holes. This could also be the reason for the lowered *FF*. Nevertheless we are not able to completely explain the *FF* variation. Therefore, measurement and characterization of real tandem structures should be conducted and compared to the simulation prediction.

3.1 Limitations of the tandem efficiency

From Figure 8, one can observe that the tandem efficiency at optimized CGS absorber thickness $W_{abs,}$ is lower than the efficiency of the single junction CIGS solar cell (depicted with the dashed line). Even if we would assume that the fill factor *FF* is constant, instead of showing a dip at $W_{abs,opt}$, the tandem efficiency would hardly surpass the efficiency of the single junction

CIGS solar cell. A too low V_{oc} value of the CGS top solar cell could be one of the reasons, if not the main reason, for this [21].

In state-of-the-art CIGS solar cells, a well known relation between the CIGS band gap E_G and the open circuit voltage V_{oc} is observed [22]

$$V_{oc} = \frac{E_G}{q} - 0.6 \text{ Volt} \tag{2}$$

where q is the electron charge. If this would also be the case with the CGS solar cell, the V_{oc} could reach a value of 1.1 V, whereas the actual V_{oc} value is limited to 800–850 mV. If this ideal value V_{oc} value of 1.1 V, and a constant FF (i.e. without a dip as in Figure 8) could be reached, we can make a rough estimation of the tandem efficiency using our model:

$$\begin{aligned} \eta &= FF \times J_{sc,M} \times \left(V_{oc,\text{CGS}} + V_{oc,\text{CIGS}}\right) \Big/ P_{AM1.5g} \\ &\approx 0.71 \times 15 \text{ mA/cm}^2 \times \left(0.6 \text{ V} + 1.1 \text{ V}\right) \Big/ 100 \text{W/cm}^2 = 18.1 \text{ \%} \end{aligned} \tag{3}$$

Although the tandem efficiency now surpasses the efficiency of the single junction CIGS used in the tandem, it is lower than the best reported single junction CIGS solar cell efficiency [23].

4. Conclusions

Simulation with a tunneling transport model at the CGS/ZnO heterointerface shows that the CGS depletion region is too wide for the tunnelling assisted recombination. A 20 nm thin, p^+–type doped interfacial layer with increased defect cross–sections is needed for an efficient recombination junction. The physical parameters of the interfacial layer point to a semi–metal. For the chosen set of the material parameters, the optimal top cell absorber thickness is around 0.2 μm. A thinner CGS absorber does not absorb enough light and the photogenerated electrons start to diffuse into the back contact. The main reason for the low tandem efficiency is a too low V_{oc} of the top CGS cell and low FF of the optimised tandem structure. For an accurate characterization of the FF loss, measurements on real structures should be conducted and compared to simulation results.

References

[1] W.H. Bloss, J. Kimmerle, F. Pfisterer, and H.W. Schock, Thin film tandem solar cells based on II–VI compounds, Proc. 17th IEEE Photovoltaic Specialists Conference (Orlando, Fla., May 1984), pp. 715–720, IEEE, Orlando (1984).

[2] S. Nishiwaki, S. Siebentritt, P. Walk, M.C. Lux–Steiner, A stacked chalcopyrite thin–film tandem solar cell with 1.2 V open–circuit voltage, *Prog. Photovolt. Res. Appl.*, **11**, 243–248 (2003).

[3] J. Song, S.L. Sheng, C.H. Huang, T.J. Anderson, and O.D. Crisalle, Modeling and simulation of a $CuGaSe_2/Cu(In_{1-x},Ga_x)Se_2$ tandem solar cell, Proc. 3rd World Conference on Photovoltaic Energy Conversion (Osaka, Japan, May 2003), pp. 555–558, WCPEC–3, Osaka (2003).

[4] D.L. Young, M. Contreras, M. Romero, S. Asher, C. Perkins, T. Gessert, J. Keane, T.J. Coutts, and R. Noufi, Interconnect junctions for thin–film tandem solar cells, Proc. 3rd World Conference on Photovoltaic Energy Conversion (Osaka, Japan, May 2003), pp. 27–30, WCPEC–3, Osaka (2003).

[5] P. Mahawela, G. Sivaraman, S. Jeedigunta, J. Gaduputi, M. Ramalingam, S. Subramanian et al., II–VI compounds as the top absorbers in tandem solar cells structures, *Mat. Sc. Eng. B*, **116**, 283–291 (2005).

[6] L. M. Woods, A. Kalla, D. Gonzales, R. Ribelin, Wide–bandgap CIAS thin–film photovoltaics with transparent back contacts for next generation single and multi–junction devices, *Mat. Sc. Eng. B*, **116**, 297–302 (2005).

[7] S. Nishiwaki, M. Dziedzina, S. Schuler, S. Siebentritt, M. Bär, A. Rumberg, M. Rusu, R. Klenk, and M.C. Lux–Steiner, Preparation of $CuGaSe_2$ solar cells and their optimization, Proc. 3rd World Conference on Photovoltaic Energy Conversion (Osaka, Japan, May 2003), pp. 471–474, WCPEC–3, Osaka (2003).

[8] F.A. Rubinelli, J. K. Rath, R.E.I. Schropp, Microcristalline n–i–p tunnel junction in a–Si:H/a–Si:H tandem cells, *J. Appl. Phys.*, **89**, 4010–4018 (2001).

[9] B.A. Mansour, M.A. El–Hagary, Transport properties of $CuGaSe_2$ thin films, *Thin Solid Films*, **256**, 165–170 (1995).

[10] D.J. Schroeder, J.L. Hernandez, G.D. Berry, A. Rockett, Hole transport and doping states in epitaxial $CuIn_{1-x}Ga_xSe_2$, *J. Appl. Phys.*, **83**, 1519–1526 (1998).

[11] U. Rau, M. Schmidt, Electronic properties of $ZnO/CdS/Cu(In,Ga)Se_2$ solar cells – aspects of heterojunction formation, *Thin Solid Films*, **387**, 141–146 (2001).

[12] R. Klenk, Characterization and modelling of chalcopyrite solar cells, *Thin Solid Films*, **387**, 135–140 (2001).

[13] A.N. Banerjee, K.K. Chattopadhyay, Recent developments in the emerging field of crystalline p–type transparent conducting oxide thin films, *Prog. in Cryst. Growth and Char. Mat.*, **50**, 52–105 (2005).

[14] P.J. Rostan, J. Matheis, G. Bilger, U. Rau, J.H. Werner, Formation of transparent and ohmic $ZnO:Al/MoSe_2$ contacts for bifacial $Cu(In,Ga)Se_2$ solar cells and tandem structures, *Thin Solid Films*, **480–481**, 67–70 (2005).

[15] T. Nakada, Microstructural and diffusion properties of CIGS thin film solar cells fabricated using transparent conducting oxide back contacts, *Thin Solid Films*, **480–481**, 419–425 (2005).

[16] G. Černivec, A. Jagomägi, F. Smole, M. Topič, Numerical and experimental indication of thermally activated tunneling transport in CIS monograin layer solar cells, *Solid State Electronics*, in revision (May 2007).

[17] N. Kohara, S. Nishiwaki, Y. Hashimoto, T. Negami, T. Wada, Electrical properties of the $Cu(In,Ga)Se_2/MoSe_2/Mo$ structure, *Sol. En. Mat. Sol. Cells*, **67**, 209–215 (2001).

[18] L. Assmann, J.C. Bernede, A. Drici, C. Amory, E. Halgand, M. Morsli, Study of the Mo thin films and Mo/CIGS interface properties, *Appl. Surf. Sc.*, **246**, 159–166 (2005).

[19] J. Krč, G. Černivec, A. Čampa, et al, Optical and electrical modelling of Cu(In,Ga)Se_2 solar cells, *Optical and Quantum Electronics*, **38**, 1115–1123 (2006).

[20] J. Krč, F. Smole, M. Topič, Analysis of light scattering in amorphous Si:H solar cells by one–dimensional semi–coherent optical model, *Prog. Photovolt.*, **11**, 15–26 (2003).

[21] S. Siebentritt, U. Rau, *Wide–Gap Chalcopyrites*, Springer, Heidelberg, 2006.

[22] G. Hanna, A. Jasenek, U. Rau, and H.W. Schock, Open Circuit Voltage Limitations in $CuIn_{1-x}Ga_xSe_2$ Thin-Film Solar Cells – Dependence on Alloy Composition, phys. stat. sol. (a), **179**, R7–R8 (2000).

[23] M.A. Contreras, K. Ramanathan, J. AbuShama, F. Hasoon et al, Diode characteristics in state of the art ZnO/CdS/Cu($In_{1-x}Ga_x$)Se_2 solar cells, *Prog. Photovolt.*, **13**, 209–216 (2005).